ACS NANO
Cite This: ACS Nano 2018, 12, 6170–6178
www.acsnano.org

ARTICLE

High-Quality In-Plane Aligned $CsPbX_3$ Perovskite Nanowire Lasers with Composition-Dependent Strong Exciton–Photon Coupling

Xiaoxia Wang,[†,§] Muhammad Shoaib,[†,§] Xiao Wang,[†,§] Xuehong Zhang,[†] Mai He,[†] Ziyu Luo,[†] Weihao Zheng,[†] Honglai Li,[†] Tiefeng Yang,[†] Xiaoli Zhu,[†] Libo Ma,[‡] and Anlian Pan*[,†]

[†]Key Laboratory for Micro-Nano Physics and Technology of Hunan Province, State Key Laboratory of Chemo/Biosensing and Chemometrics, and School of Physics and Electronics, Hunan University, Changsha, Hunan 410082, People's Republic of China
[‡]Institute for Integrative Nanosciences, Leibniz IFW Dresden, Helmholtzstraße 20, 01069 Dresden, Germany

Supporting Information

ABSTRACT: Cesium lead halide perovskite nanowires have emerged as promising low-dimensional semiconductor structures for integrated photonic applications. Understanding light–matter interactions in a nanowire cavity is of both fundamental and practical interest in designing low-power-consumption nanoscale light sources. In this work, high-quality in-plane aligned halide perovskite $CsPbX_3$ (X = Cl, Br, I) nanowires are synthesized by a vapor growth method on an annealed M-plane sapphire substrate. Large-area nanowire laser arrays have been achieved based on the as-grown aligned $CsPbX_3$ nanowires at room temperature with quite low pumping thresholds, very high quality factors, and a high degree of linear polarization. More importantly, it is found that exciton–polaritons are formed in the nanowires under the excitation of a pulsed laser, indicating a strong exciton–photon coupling in the optical microcavities made of cesium lead halide perovskites. The coupling strength in these $CsPbX_3$ nanowires is dependent on the atomic composition, where the obtained room-temperature Rabi splitting energy is ~210 ± 13, 146 ± 9, and 103 ± 5 meV for the $CsPbCl_3$, $CsPbBr_3$, and $CsPbI_3$ nanowires, respectively. This work provides fundamental insights for the practical applications of all-inorganic perovskite $CsPbX_3$ nanowires in designing light-emitting devices and integrated nanophotonic systems.

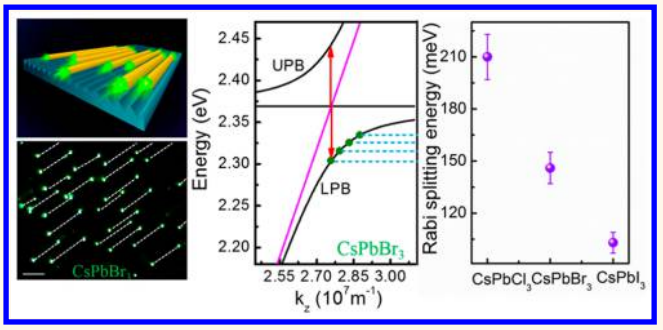

KEYWORDS: *cesium lead halide perovskite, aligned nanowires, multicolor lasers, exciton–polaritons, Rabi splitting*

Nanoscale light sources with low power consumption have been intensively pursued in the past decades for practical applications in the next-generation optoelectronic devices and nanophotonic integrated circuits.[1−9] Semiconductor nanowire lasers generated from their naturally formed Fabry–Perot (F–P) cavities have been demonstrated as a promising approach with well-defined one-dimensional geometry toward on-chip integration.[1,10−13] Since the lasing behaviors and performance of a given nanowire are largely determined by the structures and optical properties of the materials, tremendous research efforts have been devoted to discovering different types of high-quality nanowires and high-performance nanowire lasers. Recently, the emerging all-inorganic cesium lead halide perovskite ($CsPbX_3$, X = Cl, Br, I) semiconductor materials with excellent optical and thermal stabilities, high quantum yield (nearly ~90%), and low trap state were considered as potential candidates to achieve high-quality nanoscale lasing devices.[14−24] Up to now, $CsPbX_3$ perovskite nanowire lasers have been realized with low-threshold and wavelength-tunable properties, demonstrating these halide perovskite nanowires as promising candidates for on-chip lasers toward practical applications.[19,25,26]

However, the underlying physics of lasing and the light–matter interactions in perovskite nanowires are not yet well understood despite numerous reports on their performances and applications.[27−30] As is well known, the coupling between photons and excitons in semiconductor materials leads to the

Received: April 14, 2018
Accepted: June 11, 2018
Published: June 11, 2018

DOI: 10.1021/acsnano.8b02793
ACS Nano 2018, 12, 6170–6178

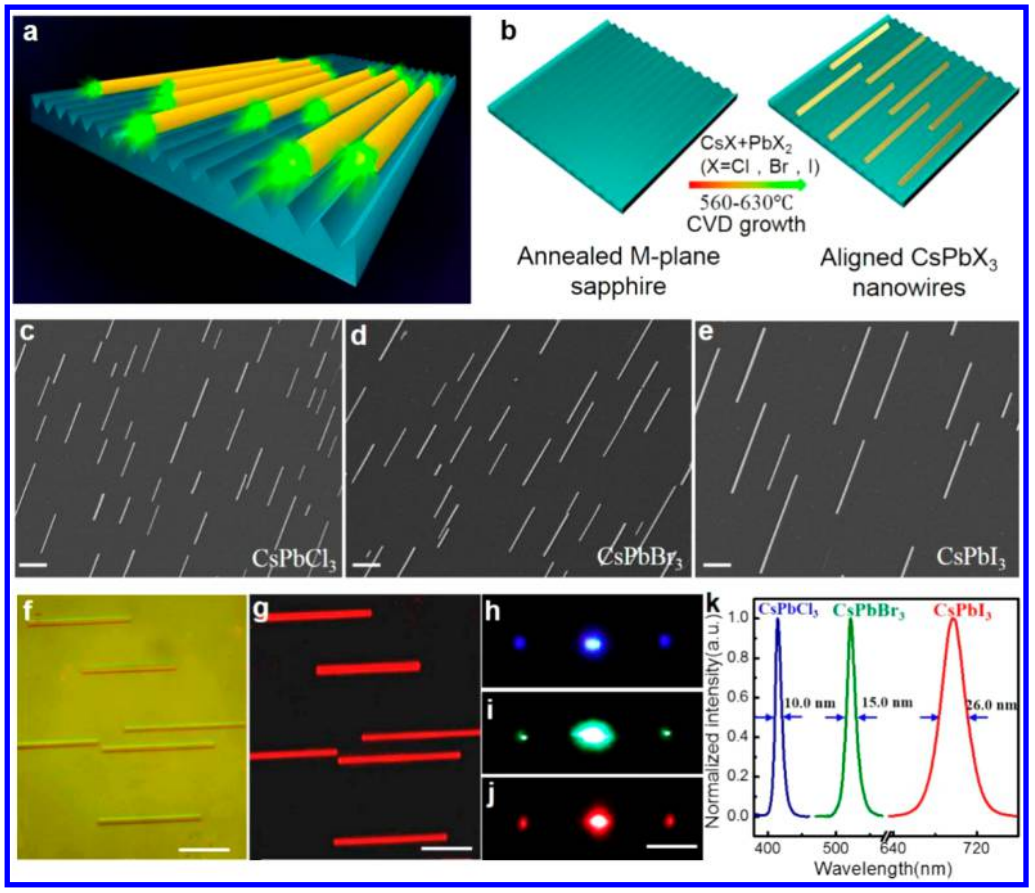

Figure 1. (a) Schematic diagram of the aligned $CsPbBr_3$ nanowire lasers. (b) Diagram of the growth process for the $CsPbX_3$ nanowires on an annealed M-plane sapphire substrate. (c–e) SEM images of the as-grown in-plane aligned $CsPbCl_3$, $CsPbBr_3$, and $CsPbI_3$ nanowires, respectively. (f) Bright-field optical image of representative $CsPbI_3$ nanowires and the corresponding real-color emission image under laser excitation (g). (h–j) Optical waveguide emission images measured from single $CsPbCl_3$, $CsPbBr_3$, and $CsPbI_3$ nanowires, respectively. (k) Normalized *in situ* photoluminescence spectra detected from single $CsPbX_3$ nanowires. Scale bar is 5 μm.

formation of exciton–polaritons which show hybrid photonic–electronic properties.[31−33] The Rabi splitting ($2g$) provides a measure of coupling strength of light–matter interaction (g), which can be expressed by the oscillator strength f and the mode volume V_m as $g \propto \sqrt{f/V_m}$. Hence, a strong coupling is usually obtained with strong oscillator strength and small mode volume. In a one-dimensional nanowire, excitonic oscillator strength is enhanced due to size effects in the synthesized high-quality nanowires and the mode volume is small due to strong confinement of resonant light in the nanowire cavity. Thus, the strengthened photon–exciton coupling facilitates the formation of cavity polaritons; for example, it has been demonstrated that the vacuum Rabi splitting in CdS and ZnO nanowires is much larger than that of macroscopic values.[31,34] Compared to conventional II–VI or III–V semiconductor nanowires, a higher density of exciton states exists in $CsPbX_3$ perovskites due to the large exciton binding energy, allowing for efficient coupling with photons to form exciton–polaritons at room temperature. In 2016, Park *et al.* investigated light–matter interactions in $CsPbX_3$ nanowires by analyzing the unusual lasing mode spacing.[26] In addition, Liu *et al.* studied strong exciton–photon coupling affected by cavity size in hybrid inorganic–organic and all-inorganic $CsPbBr_3$ perovskite micro/nanowires, similar to those reported in traditional semiconductor nanowires.[31,34−36] It is worth noting that Zhu *et al.* have very recently reported continuous wave (cw) polariton lasing in $CsPbBr_3$ nanowires with low pump intensity. They claimed that both cw and pulsed lasers originate from polariton modes due to the existence of strong exciton–photon coupling in the $CsPbBr_3$ nanowires based on the lasing mode analysis.[37] However, the chemical composition dependent exciton–photon coupling has not been systematically studied in crystalline $CsPbX_3$ perovskite nanowires, which is of high interest for not only fundamental research but also practical applications such as designing light sources and optoelectrical devices. Therefore, the systematical investigation of lasing behaviors, confined exciton–polaritons in $CsPbX_3$ nanowire cavities, and the composition-dependent Rabi splitting is highly desirable.

Here, high-quality in-plane aligned $CsPbX_3$ perovskite nanowires with a smooth surface were synthesized by a vapor growth route on annealed M-plane sapphire substrates. Wavelength-tunable aligned $CsPbX_3$ nanowire lasers were achieved at room temperature with quite low lasing thresholds, high quality factors, and a high degree of linear polarization. Furthermore, exciton–polaritons are formed in these high-quality $CsPbX_3$ (X = Cl, Br, I) perovskite nanowire cavities under the excitation of a pulsed laser. The energy–wavevector dispersion relation of the lasing mode energy is well fitted by the exciton–polariton model, from which highly composition-dependent Rabi splitting of ~210 ± 13, 146 ± 9, and 103 ± 5 meV for the $CsPbCl_3$, $CsPbBr_3$, and $CsPbI_3$ nanowires, respectively, are obtained at room temperature. Our study

DOI: 10.1021/acsnano.8b02793
ACS Nano 2018, 12, 6170–6178

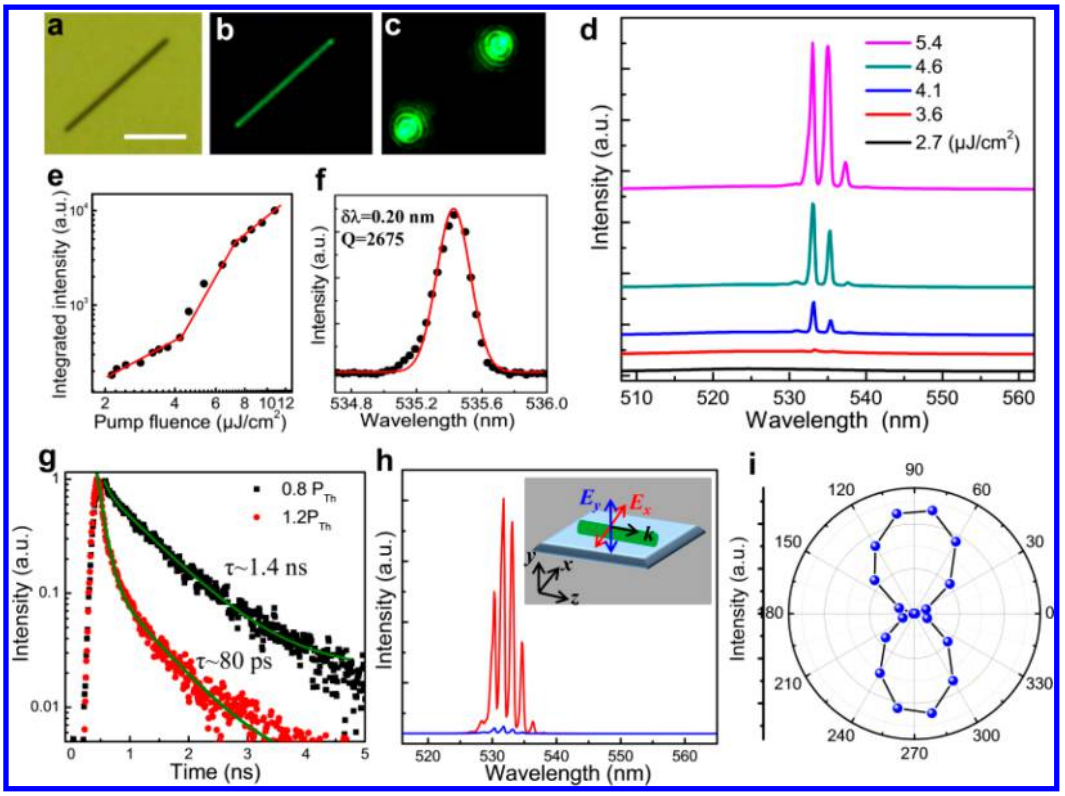

Figure 2. (a) Bright optical image of a typical $CsPbBr_3$ nanowire; scale bar is 10 μm. (b and c) Corresponding real-color optical images pumped below and above the P_{Th}, respectively. (d) Pump fluence dependent PL spectra detected from the end of the $CsPbBr_3$ nanowire in (c). (e) Log−log plot of the integrated emission intensity versus the pump fluence for the nanowire laser. (f) Gaussian fitting (red solid line) of the dominant emission mode (black dots). (g) Typical PL decay profiles of the $CsPbBr_3$ nanowire with the excitation fluence below (~$0.8P_{Th}$, black squares) and above (~$1.2P_{Th}$, red dots) the P_{Th}. (h) Lasing spectra of the nanowire for emission light electric field parallel (red arrow) and perpendicular (blue arrow) to the substrate. Inset shows the schematic of the direction relation between the emission light electric field direction and the nanowire. (i) Polar plots of integrated intensity versus detection polarization angle (φ) for the nanowire lasing spectra.

further reveals the origin of the optical gain from the achieved high-quality aligned $CsPbX_3$ nanowires, which may serve as a good model for future polaritonic investigations.

RESULTS AND DISCUSSION

Figure 1a shows the schematic diagram of the in-plane aligned halide perovskite nanowire lasers. These directional perovskite nanowires were synthesized by a simple vapor growth route. The process is schematically shown in Figure 1b. Due to the thermodynamically unstable M-plane sapphire surface, it forms V-shaped nanogroove structures (left side of Figure 1b) upon high-temperature annealing.[38] The width and depth of these nanogrooves are ~80 nm and ~13 nm, respectively, as confirmed by atomic force microscopy (AFM) (see Figure S1). After starting the growth, the mixture of CsX and PbX_2 (X = Cl, Br, I) vapor precursor will deposit and nucleate at the surface of sapphire due to van der Waals epitaxy. These initial nucleating clusters can serve as seeds to grow into one-dimensional nanostructures, as described in previous work.[39,40] The existence of the nanogrooves at the substrate surface will guide the growth of these wires to finally form in-plane well-aligned nanowires, as shown on the right in Figure 1b.

A detailed morphology investigation of the as-grown nanowires was conducted using scanning electron microscopy (SEM). Figure 1c shows a SEM image of the as-grown $CsPbBr_3$ nanowire sample, which exhibits a large area and a high density of directionally assembled nanowires. The local high-magnification SEM investigation of single $CsPbBr_3$ nanowires shows that the wires are parallel to the length direction of the nanogrooves on the annealed sapphire substrate, with a very smooth surface, uniform element distribution, and a well-defined triangular cross-section (see Figure S2). The formation of these triangular cross-section nanowires is thermodynamically favorable, the details of which have been described in our latest work.[39] By changing the kinds of evaporation sources and adjusting the deposition temperature, aligned $CsPbCl_3$ and $CsPbI_3$ nanowires were also obtained, as shown in Figure 1d and e. From the results, it is found that these nanowires are straight and grow parallel along the same direction with an average length of about 10−20 μm and a diameter of 200−500 nm. In addition, optical images and X-ray diffraction (XRD) characterizations all demonstrate that in-plane aligned $CsPbCl_3$, $CsPbBr_3$, and $CsPbI_3$ nanowires are all successfully synthesized by the vapor method on an annealed sapphire substrate (see Figures S3−S5).

We next studied the basic photoluminescence (PL) properties of these as-grown $CsPbX_3$ nanowires. Figure 1f and g show the bright-field optical image of the aligned $CsPbI_3$ nanowires and the corresponding real-color emission image under broad laser excitation. It is clearly found that the red color originating from band edge spontaneous emission is distributed homogeneously in each nanowire, which reveals the high crystalline quality of these $CsPbI_3$ nanowires. Figure 1h,i further give the optical waveguide of single $CsPbCl_3$, $CsPbBr_3$,

DOI: 10.1021/acsnano.8b02793
ACS Nano 2018, 12, 6170−6178

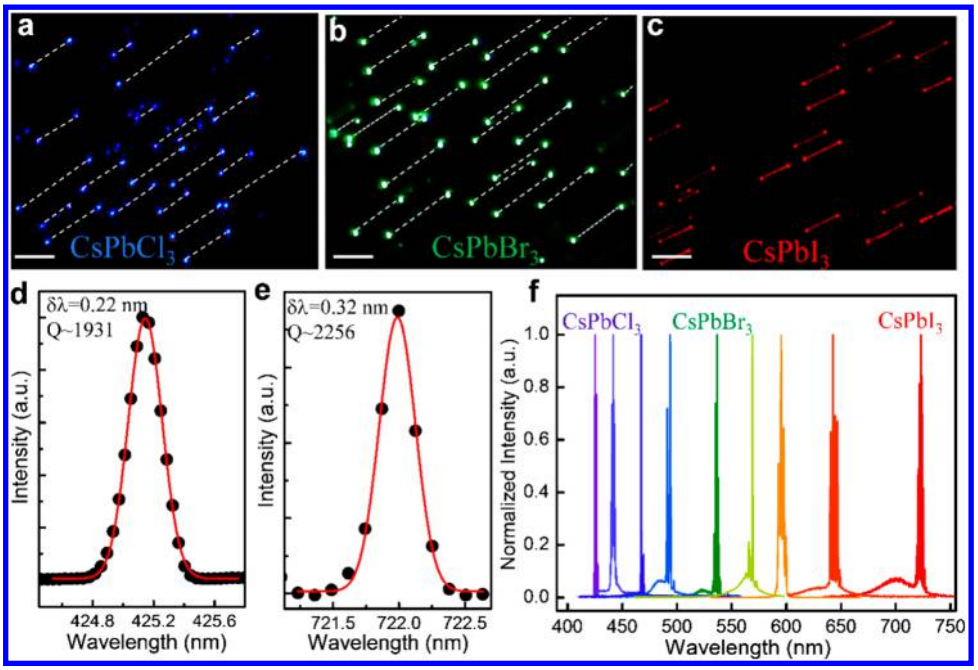

Figure 3. (a–c) Real-color optical images of the in-plane directional $CsPbCl_3$, $CsPbBr_3$, and $CsPbI_3$ nanowire assembles under optical pumping above their lasing thresholds. Scale bar is 10 μm. Dashed lines in (a) and (b) indicate the locations of the wires. (d and e) Gaussian fitting of the dominant mode extracted from the lasing spectra detected from $CsPbCl_3$ and $CsPbI_3$ nanowires. (f) Broad wavelength tunable lasing spectra from the directional $CsPbX_3$ and alloy nanowires.

and $CsPbI_3$ nanowires, respectively, under localized laser excitation at the middle of the nanowire. The three compositions all show excellent waveguide properties with bright light emitted from both ends of the nanowires with low optical propagation loss (see Figure S6). The corresponding room-temperature *in situ* normalized PL spectra detected from a single nanowire show very narrow full widths at half-maximum (fwhm) of ~10.0, ~15.0, and ~26.0 nm for $CsPbCl_3$, $CsPbBr_3$, and $CsPbI_3$ nanowires, respectively (Figure 1k). The fwhm of the as-grown aligned $CsPbX_3$ nanowires is much smaller than that of reported colloidal $CsPbX_3$ quantum dots (12.0–40.0 nm) and $CsPbX_3$ nanoplatelets (8.0–30.0 nm), which implies high exciton binding energy and low defects of these $CsPbX_3$ nanowires.[20,21] The above results confirm that high-quality in-plane aligned $CsPbX_3$ nanowires have been achieved on the annealed M-plane sapphire.

Lasing behaviors of the as-grown in-plane directional $CsPbX_3$ nanowires were examined at room temperature. Figure 2a shows the optical image of a representative single $CsPbBr_3$ nanowire (length is ~10 μm, diameter is 300 nm). When the nanowire is pumped with low excitation density, uniform and bright green spontaneous emission (SPE) is observed from the whole $CsPbBr_3$ wire (Figure 2b). As the excitation fluence increases above the P_{Th}, stimulated emission (SE) dominates, strong lasing emission with spatial interference patterns from the two coherent sources at the ends of the nanowire, as shown in Figure 2c. The bright emission localized at the two ends arises from the low-loss optical waveguiding effect and axial F–P resonator modes (see Figure S6). Almost no light emission is observed from the body of the wires at high pump intensity due to the high degree of coupling of the spontaneous emission to the cavity oscillation modes, which further demonstrates the high crystalline quality and nearly perfect end facets of the as-grown $CsPbBr_3$ nanowire.[10] The excitation fluence dependent photoluminescence spectrum is shown in Figure 2d. A broad spontaneous emission spectrum was observed with the peak centered at 525 nm under low-fluence pumping (2.7 μJ cm^{-2}). Significantly, once the pump fluence was enhanced to ~3.6 μJ cm^{-2}, a series of narrow peaks appeared at the low energy edge of the spontaneous emission band, and the intensity grows rapidly with further increasing the excitation fluence, indicating the lasing action of the $CsPbBr_3$ nanowires. For single $CsPbCl_3$ and $CsPbI_3$ nanowires, optically pumped F–P cavity lasers are also realized at room temperature (see Figures S7 and S8). These results demonstrate that these as-grown $CsPbX_3$ nanowires can work as efficient optical waveguides to achieve high-quality lasers.

Figure 2e shows the excitation fluence dependent output intensity of the guided nanowires, which follows a typical nonlinear "S"-curve shape and gives a threshold of ~4 μJ cm^{-2}. The result further reveals the transition from spontaneous emission *via* amplified spontaneous emission to finally stimulated radiation with increasing excitation fluence. It is noted that the fwhm ($\delta\lambda$) of the dominating lasing mode at 535 nm is only ~0.20 nm (fitted by a Gaussian function, Figure 2f), which corresponds to an estimated quality factor of ~2256 calculated by using the relationship $Q = \lambda/\delta\lambda$. The quality factor of the nanowire is higher than that of the reported $CsPbX_3$ nanowires synthesized by a vapor growth method,[26] indicating the high quality of the achieved in-plane aligned $CsPbX_3$ nanowires.

To demonstrate the dynamic process of the lasing action, time-resolved photoluminescence (TRPL) spectroscopy of single $CsPbBr_3$ nanowires is performed by a streak-camera system. Figure 2g shows the TRPL decay curves at different excitation fluences spanning from SPE to SE processes. As pumped with low-excitation fluences (~0.8P_{Th}, black squares), the SPE decay profile fitted by an exponential function yields a lifetime of τ_{SPE} = 1.4 ns, while a very fast decay time of ~80 ps

DOI: 10.1021/acsnano.8b02793
ACS Nano 2018, 12, 6170–6178

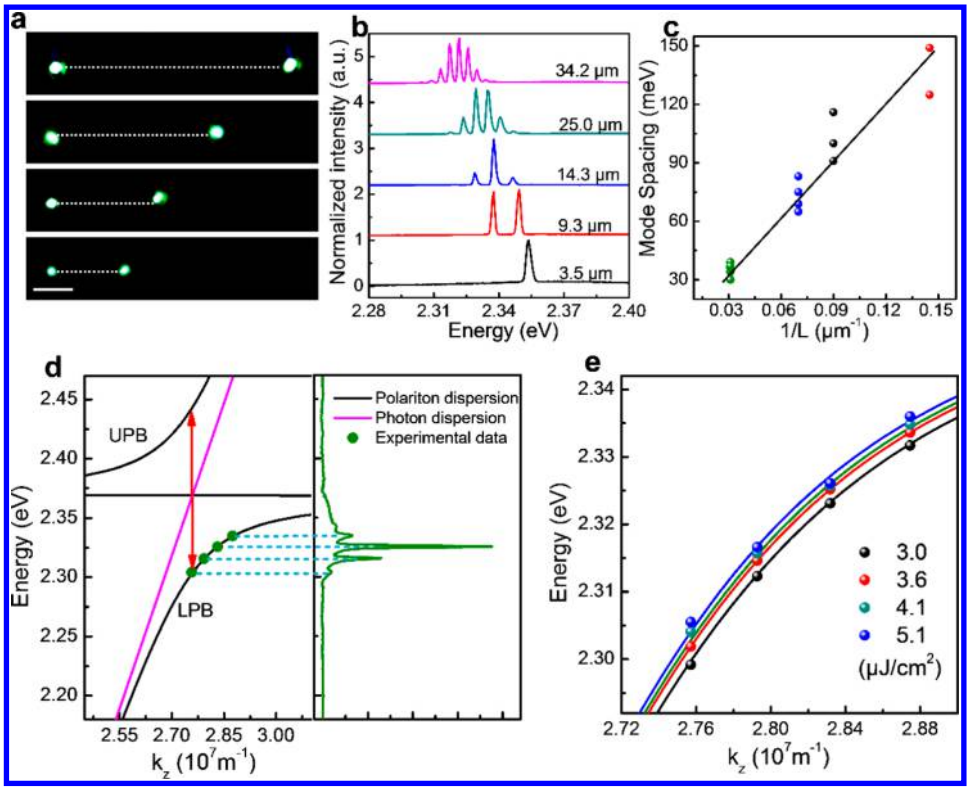

Figure 4. (a) Real-color optical images of $CsPbBr_3$ nanowires with different length pumped above the P_{Th}. Scale bar is 5 μm. (b) Lasing spectra recorded for different length nanowires. (c) Plot of mode spacings as a function of the inverse of the nanowire length. The solid line is the linear least-squares fitting. (d) Left panel: plot of photon energy−wavevector (E−k) dispersion (pink line) and the exciton−polariton E−k dispersion (black line) curves for the wire with a length of ~10 μm. The green scatter dots represent the lasing peaks' energy (corresponding to the spectra in the right panel) that can be fitted by the exciton−polariton model. The red arrow indicates the Rabi splitting. (e) Pump fluence dependent energy−wavevector dispersion curves of the same wire used in (d).

is obtained when the excitation fluence is above the threshold (~1.2P_{Th}, red dots), also indicating the occurrence of a stimulated emission process and lasing action with the $CsPbBr_3$ nanowire cavity. Further analysis demonstrated that the achieved $CsPbBr_3$ nanowire lasers have a very high degree of linear polarization. Figure 2h shows the polarization-dependent spectra for the lasing when the electric field of emission light is separately parallel (E_x, red curves) and perpendicular (E_y, blue curves) to the substrate, as shown schematically in the inset of Figure 2h. The zero degree of the polarization detection angle is defined as the direction parallel to E_y. It is clearly found that the polarization of the lasing mode exhibits a maximizing value (I_{max}) in the E_x component (red) and minimizing (I_{min}) in the E_y component (blue). The polarization relationship of the lasing emission is further demonstrated by the detection polarization angle (φ) dependent integrated intensities (Figure 2i). The result is plotted in polar coordinates with the maximum value at ~90°. We define the degree of polarization (DOP) as DOP = $(I_{max} - I_{min})/(I_{max} + I_{min})$, and from the formula the DOP is calculated as 98%, which demonstrates the high degree of linear polarization of the $CsPbBr_3$ nanowire lasers. The polarization of the lasing emission is determined by the modes coupled to the lasing cavity and is further confirmed by the numerical simulation results (see Figure S9). Clearly, the polarization of the electric field at the fundamental mode is dominant in the width (x) direction with a very weak component in the length (y) and thickness (z) direction, which agrees well with the experimental results.

Due to the high quality and uniformity of the as-grown nanowires, simultaneous laser operation can be achieved from aligned $CsPbX_3$ nanowire assembles. Figure 3a−c show the real-color optical images of the nanowires under the broad illumination of a femtosecond pulse laser at 400 nm for $CsPbCl_3$ and 470 nm for $CsPbBr_3$ and $CsPbI_3$ above their thresholds. It is found from Figure 3a−c that bright light emits from the two ends of all these directional $CsPbX_3$ nanowires, confirming the realization of high-quality in-plane aligned $CsPbX_3$ nanowire lasing action. More importantly, the blue ($CsPbCl_3$), green ($CsPbBr_3$), and red ($CsPbI_3$) laser emissions comprise basic components of three primary colors, which will be beneficial for white light emitting devices and full color displays. Figure 3d and e are the zoom-in of dominant lasing modes for $CsPbCl_3$ and $CsPbI_3$ nanowires, respectively. The lasing peaks are well fitted by a Gaussian function with fwhms of 0.22 and 0.32 nm, yielding a quality factor of ~1931 and ~2256 for $CsPbCl_3$ and $CsPbI_3$ nanowires, respectively. To further extend the application of the in-plane directional nanowire lasers, multicolor nanolasers are realized based on the controllable chemical stoichiometry of perovskites. Figure 3f shows the broad-wavelength-tunable lasing spectra detected from directional $CsPb(Cl_xBr_{1-x})_3$ and $CsPb(Br_xI_{1-x})_3$ nanowires at room temperature, ranging from 425 to 722 nm, almost covering the whole visible light region. The above results further confirm the realization of high-quality and multicolor perovskite nanowire lasers through the in-plane directional growth approach.

DOI: 10.1021/acsnano.8b02793
ACS Nano 2018, 12, 6170−6178

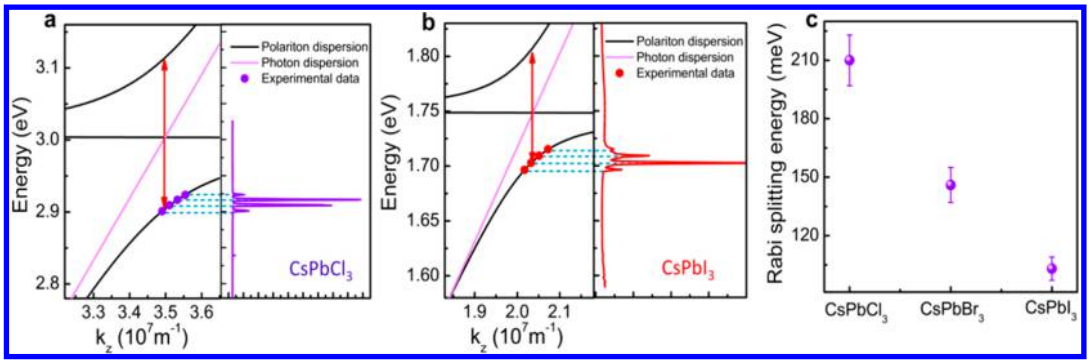

Figure 5. (a, b) Energy−wavevector dispersion curves of the lasing peaks' energy fitted by the exciton−polariton model for the $CsPbCl_3$ and $CsPbI_3$ nanowires, respectively. (c) Rabi splitting energy for the $CsPbCl_3$, $CsPbBr_3$, and $CsPbI_3$ nanowires with the same length (~10 μm). The error bars are derived from the changing of oscillator strength of the nanowire cavity when pumped with different excitation intensity.

In addition to the excellent lasing characteristics, we now focus on the investigation of the origin of lasing modes and the light−matter interactions in these nanowires. To experimentally investigate the progression of exciton−photon interactions and the coupling strength in these directional $CsPbX_3$ nanowires, we extract the lasing mode energy to construct the energy−wave vector dispersions.[12,41] We first check the lasing modes and their mode spacing from several $CsPbBr_3$ nanowires. Figure 4a shows the real-color dark-field optical images of $CsPbBr_3$ nanowires with different lengths pumped above their P_{Th}. Bright light spots emit from both ends of each wire, which indicates lasing action occurs with these wires. The corresponding lasing modes are recorded and shown in Figure 4b. It is found that the lasing spectra change from single mode to multimode and the modes' wavelengths shift continuously from ~527 nm (2.35 eV) to ~534 nm (2.32 eV) with the length (L) increasing from 3.5 μm to 34.2 μm. This red shifting comes from the band tail state induced self-absorption of the guided light in the nanowire cavities.[42,43] Figure 4c shows the inverse of length-dependent mode spacing for four nanowires. The mode spacing is linear inversely to the length of these guided wires, which is consistent with the F−P-like lasing mode characteristics. However, in contrast to the classical pure photonic model in the F−P cavity, it is noted that the mode spacing decreases with increasing mode number for a given nanowire (see Figure S10). This unusual mode spacing is expected from the occurrence of exciton−photon coupling induced formation of polaritons in the anticrossing negative curvature low polariton branches.[37]

To quantitatively analyze the exciton−polariton dispersion and the Rabi splitting of the polariton branches in the $CsPbBr_3$ nanowires, we use the exciton−photon coupling model, where the energy of the polaritons is defined by the equation[12]

$$E(w, k) = \frac{\hbar c k}{\sqrt{\varepsilon(w, k)}} \tag{1}$$

where $\hbar$ represents the reduced Plank constant, c is the velocity of light in a vacuum, k is the wave vector, w is the frequency of the exciton−polaritons, and $\varepsilon(w, k)$ is the dielectric function of the material, which varies as the frequency w. Hence the dielectric function $\varepsilon(w, k)$ determines the energy−wave vector dispersion relation of exciton−polaritons. According to the dielectric function of a microscopic model, $\varepsilon(w, k)$ of the nanowire cavity is then given by[12,44,45]

$$\varepsilon(w, k) = \varepsilon_b\left(1 + \Omega\frac{f}{w_T^2 - w^2}\right) = \frac{c^2}{w^2}k_z^2 \tag{2}$$

$$k_z = m\frac{\pi}{L_z} + k_0 \tag{3}$$

where ε_b is the background dielectric constant, Ω is a prefactor, and f is the oscillator strength of the nanowire cavity, which is defined by the transverse (w_T) and longitudinal (w_L) resonance frequencies ($f = w_L^2 - w_T^2$). k_0 represents the wave vector of the lowest energy mode, which can be regarded as a fitting parameter together with f.

Considering the exciton−polariton dispersion, the energies of these lasing peaks with different mode spacing are equally spaced at an integer number of π/L_z (L_z, wire length) in the wave vector space. Thus, when the lasing peak energy is plotted versus incremental wave vector multiples of π/L_z according to eqs 2 and 3, the shape of the energy−wave vector dispersion and the Rabi splitting energy can be determined by eq 1.[46,47] Figure 4d shows the photonic mode dispersion (pink line) and the polariton dispersion curve (black line) in the $CsPbBr_3$ nanowire cavity with a length of ~10 μm. The energy of the lasing peaks (green scatter dots) is well fitted by the exciton−polariton model and situated on the lower polariton branch, as shown in the left panel of Figure 4d. It is worth mentioning that the exciton−photon coupling only occurs in the lower energy range, which is ascribed to the large scattering and absorption loss of higher energy photons due to the intrinsic existence of an Urbach tail in the semiconductor nanowires.[42] The fitting yields a room-temperature Rabi splitting energy of ~146 meV. The obtained large Rabi splitting of the $CsPbBr_3$ nanowire reveals the existence of strong light−matter interaction of the aligned $CsPbBr_3$ nanowire, which is mainly attributed to the large oscillator strength of the confined nanowire cavity and large exciton binding energy of this class of materials at room temperature. Indeed, the reasons for the large Rabi splitting of the perovskite nanowire are complex. Many factors will impact the Rabi splitting energy for a nanoscale structure such as carrier densities, crystalline quality, and the dimension of the cross-sections.[31,41,44,47] Figure 4e shows the energy−wave-vector relations of the lasing modes with the increasing of pump fluence. It is found that each mode shifts gradually to high energy and can be well fitted with the exciton−polariton model, indicating the light−matter interaction is preserved at high pump fluence. However, the fitting $E-k$ curves show that

DOI: 10.1021/acsnano.8b02793
ACS Nano 2018, 12, 6170−6178

the oscillator strength (f) of the nanowire decreased ~10% at a pump fluence of 5.1 $\mu J/cm^2$ compared with that pumped at a low fluence of ~3.0 $\mu J/cm^2$, which is attributed to the reduced exciton binding energy by free carrier screening.[12,44] Thus, the exciton−photon coupling strength is also weakened and yields Rabi splitting ranging from 137 to 155 meV for the same wire at different pump fluences above the P_{Th}. The above results also demonstrate that the lasing modes exhibit a hybrid of photonic and polariton mode characteristics due to the occurrence of strong exciton−photon coupling in the nanowire cavity.

We further investigate the composition-dependent exciton−photon coupling of the aligned $CsPbX_3$ nanowires, and their Rabi splitting energies are also quantitatively obtained by the exciton−photon coupling model. Figure 5a and b show the fitted energy−wavevector dispersion relations of the modes; energy extracted from lasing spectra for single $CsPbCl_3$ and $CsPbI_3$ nanowires. From these results, we obtained a Rabi splitting of ~103 and ~210 meV for $CsPbI_3$ and $CsPbCl_3$ nanowires, respectively. Figure 5c further plots the statistics result of Rabi splitting of the three representative composition $CsPbX_3$ (X = Cl, Br, I) nanowires with a similar cavity geometry (length ~10 μm, diameter ~300 nm). The result indicates a large difference in the exciton-coupling strength for the three compositions. Generally, the exciton−photon coupling strength of a given nanowire is mainly affected by the cavity oscillator strength and the exciton binding energy of the material. The quality factor of the nanowire for the three compositions is demonstrated in the same range with a value of ~2000, as shown in Figures 2 and 3. The exciton binding energy of $CsPbCl_3$, $CsPbBr_3$, and $CsPbI_3$ crystals is reported to be ~72, ~40, and ~20 meV, respectively.[20,21] Generally, a larger exciton binding energy implies higher density exciton states against the free carriers when the nanowire is excited with a laser, which enables strong coupling with the confined photons in the nanowire cavity, leading to a larger Rabi splitting energy.[34,45] In addition, the obtained Rabi splitting is comparable to the values from $CsPbBr_3$ nanowires by the solution method and $CsPbCl_3$ nanoplates in distributed Bragg reflectors.[37,48] Although these dispersion curves are fitted with parameters from bulk samples, which might yield the obtained Rabi splitting energy with possible errors, our analysis provides a convincing composition-dependent Rabi splitting variation tendency. This result experimentally demonstrates that the exciton−photon coupling strength of $CsPbX_3$ perovskite nanowires is highly composition dependent and reveals the strong room-temperature light−matter interactions in the photon-confined $CsPbX_3$ nanowire cavities.

CONCLUSIONS

In summary, high-quality in-plane aligned $CsPbX_3$ perovskite nanowires were synthesized *via* a vapor growth method on an annealed sapphire substrate with very smooth surfaces and uniform size. The nanowires themselves can act as efficient gain mediums and low-loss optical cavities, based on which multicolor aligned nanolasers are achieved with very low lasing threshold, high quality factor, and high degree of linear polarizations at room temperature. More importantly, exciton−polaritons are formed and investigated under the pulsed laser excitation from these aligned $CsPbX_3$ nanowires. We fitted the energy−wavevector dispersion of the detected lasing mode energy using the exciton−photon coupling model, which shows a large Rabi splitting energy of 210 ± 13, 146 ± 9, and 103 ± 5 meV for the $CsPbCl_3$, $CsPbBr_3$, and $CsPbI_3$ nanowires, respectively. This work makes an important step toward miniaturized nanolasers and provides fundamental insight into light−matter interactions in $CsPbX_3$ peroviskites nanowires. More interestingly, the cavity polariton formation may lead to the observation of a Bose−Einstein condensate, which is of fundamental significance for the realization of a low-threshold continuous-wave polariton laser.

METHODS

Synthesis of the In-Plane Directional Nanowires. M-plane sapphire was annealed at 1400 °C for 10 h with ambient air protection. Prior to use, the substrates were sonicated for 10 min in acetone, 10 min in isopropyl alcohol, and 10 min in distilled H_2O and blow-dried in N_2. $CsPbX_3$ guided nanowires were synthesized based on the thermal evaporation of CsX and PbX_2. First, a mixture of CsX and PbX_2 powders were placed at the center of a heating zone with a molar ratio of 1:1. Several pieces of annealed M-plane sapphire substrates were placed on the alumina boat at the downstream. High-purity N_2 gas was introduced into the quartz tube with a constant flowing rate (60 sccm) to purge the O_2. Then the furnace was rapidly heated to 560−630 °C and maintained at this temperature for 30 min, keeping the pressure inside the tube at 250−300 Torr. Semiconductor $CsPbX_3$ products were deposited on the surface of the sapphire substrate at the deposition temperature of 300−400 °C. After the growth, a large number of directional nanowires on the sapphire surface were obtained.

Optical Characterization. The optical properties were measured with the confocal μ-PL system (WITec, alpha-300). A 488 nm CW laser was used as the excitation source for PL and waveguide measurements of the $CsPbBr_3$ nanowires. The laser was introduced to the confocal system and focused onto the samples through a 10× objective from the bottom of the samples. The *in situ* PL signals and waveguide emission were collected by another 100× objective and detected by a spectrometer (300 g/mm grating). A Spectra Physics Ti:sapphire laser at 470 nm (100 fs, 1 kHz) was used for $CsPbBr_3$ and $CsPbI_3$ nanowire lasing measurements, while the $CsPbCl_3$ nanowire is pumped with a 400 nm (100 fs, 1 kHz) wavelength laser. The excitation light sources are obliquely focused to the sample by a lens. The real-color images of these large-area in-plane aligned lasers are taken by a CCD camera, and the corresponding laser spectra are also detected by a spectrometer. TRPL is measured by a streak camera (Hasmamatsu Universal, C10910) with a resolution of ~80 ps for a long time range mode of about 5 ns. All experiments were performed at room temperature.

ASSOCIATED CONTENT

Supporting Information

The Supporting Information is available free of charge on the ACS Publications website at DOI: 10.1021/acsnano.8b02793.

AFM images of the substrate, XRD spectra, optical and SEM images, single-nanowire optical waveguide and the loss, laser spectra for $CsPbCl_3$ and $CsPbI_3$ nanowires, numerical simulation, and the unusual lasing mode spacing (PDF)

AUTHOR INFORMATION

Corresponding Author

*E-mail: anlian.pan@hnu.edu.cn.

ORCID

Xiao Wang: 0000-0002-2973-8215
Honglai Li: 0000-0002-4321-1807
Libo Ma: 0000-0001-9850-2292
Anlian Pan: 0000-0003-3335-3067

DOI: 10.1021/acsnano.8b02793
ACS Nano 2018, 12, 6170−6178

Author Contributions

[§]X. Wang, M. Shoaib, and X. Wang contributed equally.

Notes

The authors declare no competing financial interest.

ACKNOWLEDGMENTS

The authors are grateful to the NSF of China (Nos. 51525202, 51772084, 61574054, 61505051, and 61635001), the Hunan Province Science and Technology Plan (Nos. 2014FJ2001 and 2014TT1004), the Aid Program for Science and Technology Innovative Research Team in Higher Educational Institutions of Hunan Province, and the Fundamental Research Funds for the Central Universities.

REFERENCES

(1) Lieber, C. M. Semiconductor Nanowires: A Platform for Nanoscience and Nanotechnology. *MRS Bull.* **2011**, *36*, 1052−1063.
(2) Oulton, R. F.; Sorger, V. J.; Zentgraf, T.; Ma, R. M.; Gladden, C.; Dai, L.; Bartal, G.; Zhang, X. Plasmon Lasers at Deep Subwavelength Scale. *Nature* **2009**, *461*, 629.
(3) Suematsu, Y. Advances in Semiconductor Lasers. *Phys. Today* **1985**, *38*, 32−39.
(4) Zhang, Q.; Su, R.; Du, W.; Liu, X.; Zhao, L.; Ha, S. T.; Xiong, Q. Advances in Small Perovskite-Based Lasers. *Small Methods.* **2017**, *1*, 1700163.
(5) Guo, P.; Zhuang, X.; Xu, J.; Zhang, Q.; Hu, W.; Zhu, X.; Wang, X.; Wan, Q.; He, P.; Zhou, H.; Pan, A. Low-Threshold Nanowire Laser Based on Composition-Symmetric Semiconductor Nanowires. *Nano Lett.* **2013**, *13*, 1251−1256.
(6) Xu, J.; Zhuang, X.; Guo, P.; Zhang, Q.; Huang, W.; Wan, Q.; Hu, W.; Wang, X.; Zhu, X.; Fan, C. Wavelength-Converted/Selective Waveguiding Based on Composition-Graded Semiconductor Nanowires. *Nano Lett.* **2012**, *12*, 5003−5007.
(7) Zhuang, X.; Ning, C. Z.; Pan, A. Composition and Bandgap-Graded Semiconductor Alloy Nanowires. *Adv. Mater.* **2012**, *24*, 13−33.
(8) Zhu, H.; Fu, Y.; Meng, F.; Wu, X.; Gong, Z.; Ding, Q.; Gustafsson, M. V.; Trinh, M. T.; Jin, S.; Zhu, X. Y. Lead Halide Perovskite Nanowire Lasers with Low Lasing Thresholds and High Quality Factors. *Nat. Mater.* **2015**, *14*, 636−642.
(9) Fu, Y.; Zhu, H.; Schrader, A. W.; Liang, D.; Ding, Q.; Joshi, P.; Hwang, L.; Zhu, X.; Jin, S. Nanowire Lasers of Formamidinium Lead Halide Perovskites and Their Stabilized Alloys with Improved Stability. *Nano Lett.* **2016**, *16*, 1000.
(10) Johnson, J. C.; Yan, H.; Yang, P.; Saylcally, R. J. Optical Cavity Effects in ZnO Nanowire Lasers and Waveguides. *J. Phys. Chem. B* **2003**, *107*, 8816−8828.
(11) Saxena, D.; Mokkapati, S.; Parkinson, P.; Jiang, N.; Gao, Q.; Tan, H. H.; Jagadish, C. Optically Pumped Room-Temperature GaAs Nanowire Lasers. *Nat. Photonics* **2013**, *7*, 963−968.
(12) Vanmaekelbergh, D.; van Vugt, L. K. ZnO Nanowire Lasers. *Nanoscale* **2011**, *3*, 2783−2800.
(13) Yan, R.; Gargas, D.; Yang, P. Nanowire Photonics. *Nat. Photonics* **2009**, *3*, 569−576.
(14) Beal, R. E.; Slotcavage, D. J.; Leijtens, T.; Bowring, A. R.; Belisle, R. A.; Nguyen, W. H.; Burkhard, G. F.; Hoke, E. T.; McGehee, M. D. Cesium Lead Halide Perovskites with Improved Stability for Tandem Solar Cells. *J. Phys. Chem. Lett.* **2016**, *7*, 746−751.
(15) Swarnkar, A.; Chulliyil, R.; Ravi, V. K.; Irfanullah, M.; Chowdhury, A.; Nag, A. Colloidal CsPbBr3 Perovskite Nanocrystals: Luminescence beyond Traditional Quantum Dots. *Angew. Chem.* **2015**, *127*, 15644−15648.
(16) Wang, X.; Zhou, H.; Yuan, S.; Zheng, W.; Jiang, Y.; Zhuang, X.; Liu, H.; Zhang, Q.; Zhu, X.; Wang, X.; Pan, A. L. Cesium Lead Halide Perovskite Triangular Nanorods as High-Gain Medium and Effective Cavities for Multiphoton-Pumped Lasing. *Nano Res.* **2017**, *10*, 3385−3395.
(17) Zhang, D.; Eaton, S. W.; Yu, Y.; Dou, L.; Yang, P. Solution-Phase Synthesis of Cesium Lead Halide Perovskite Nanowires. *J. Am. Chem. Soc.* **2015**, *137*, 9230−3.
(18) Zhang, D.; Yang, Y.; Bekenstein, Y.; Yi, Y.; Gibson, N. A.; Wong, A. B.; Eaton, S. W.; Kornienko, N.; Qiao, K.; Lai, M. Synthesis of Composition Tunable and Highly Luminescent Cesium Lead Halide Nanowires through Anion-Exchange Reactions. *J. Am. Chem. Soc.* **2016**, *138*, 7236−7239.
(19) Eaton, S. W.; Lai, M.; Gibson, N. A.; Wong, A. B.; Dou, L.; Ma, J.; Wang, L. W.; Leone, S. R.; Yang, P. Lasing in Robust Cesium Lead Halide Perovskite Nanowires. *Proc. Natl. Acad. Sci. U. S. A.* **2016**, *113*, 1993−1998.
(20) Zhang, Q.; Su, R.; Liu, X.; Xing, J.; Sum, T. C.; Xiong, Q. High-Quality Whispering-Gallery-Mode Lasing from Cesium Lead Halide Perovskite Nanoplatelets. *Adv. Funct. Mater.* **2016**, *26*, 6238−6245.
(21) Protesescu, L.; Yakunin, S.; Bodnarchuk, M. I.; Krieg, F.; Caputo, R.; Hendon, C. H.; Yang, R. X.; Walsh, A.; Kovalenko, M. V. Nanocrystals of Cesium Lead Halide Perovskites ($CsPbX_3$, X = Cl, Br, and I): Novel Optoelectronic Materials Showing Bright Emission with Wide Color Gamut. *Nano Lett.* **2015**, *15*, 3692.
(22) Yakunin, S.; Protesescu, L.; Krieg, F.; Bodnarchuk, M. I.; Nedelcu, G.; Humer, M.; De, L. G.; Fiebig, M.; Heiss, W.; Kovalenko, M. V. Low-Threshold Amplified Spontaneous Emission and Lasing from Colloidal Nanocrystals of Caesium Lead Halide Perovskites. *Nat. Commun.* **2015**, *6*, 1−8.
(23) Wang, Y.; Sun, X.; Shivanna, R.; Yang, Y.; Chen, Z.; Guo, Y.; Wang, G. C.; Wertz, E.; Deschler, F.; Cai, Z. Photon Transport in One-Dimensional Incommensurately Epitaxial CsPbX3 Arrays. *Nano Lett.* **2016**, *16*, 7974.
(24) Chen, J.; Fu, Y.; Samad, L.; Dang, L.; Zhao, Y.; Shen, S.; Guo, L.; Song, J. Vapor-Phase Epitaxial Growth of Aligned Nanowire Networks of Cesium Lead Halide Perovskites ($CsPbX_3$, X = Cl, Br, I). *Nano Lett.* **2017**, *17*, 460.
(25) Fu, Y.; Zhu, H.; Stoumpos, C. C.; Ding, Q.; Wang, J.; Kanatzidis, M. G.; Zhu, X.; Jin, S. Broad Wavelength Tunable Robust Lasing from Single-Crystal Nanowires of Cesium Lead Halide Perovskites (CsPbX3, X = Cl, Br, I). *ACS Nano* **2016**, *10*, 7963−7972.
(26) Park, K.; Lee, J. W.; Kim, J. D.; Han, N. S.; Jang, D. M.; Jeong, S.; Park, J.; Song, J. K. Light-Matter Interactions in Cesium Lead Halide Perovskite Nanowire Lasers. *J. Phys. Chem. Lett.* **2016**, *7*, 3703.
(27) Fraser, M. D.; Höfling, S.; Yamamoto, Y. Physics and Applications of Exciton-Polariton Lasers. *Nat. Mater.* **2016**, *15*, 1049.
(28) Sanvitto, D.; Kénacohen, S. The Road Towards Polaritonic Devices. *Nat. Mater.* **2016**, *15*, 1061−1073.
(29) Byrnes, T.; Na, Y. K.; Yamamoto, Y. Exciton-Polariton Condensates. *Nat. Phys.* **2014**, *10*, 803−813.
(30) Christopoulos, S.; von Högersthal, G. B.; Grundy, A. J.; Lagoudakis, P. G.; Kavokin, A. V.; Baumberg, J. J.; Christmann, G.; Butté, R.; Feltin, E.; Carlin, J. F. Room-Temperature Polariton Lasing in Semiconductor Microcavities. *Phys. Rev. Lett.* **2007**, *98*, 126405.
(31) van Vugt, L. K.; Piccione, B.; Cho, C. H.; Nukala, P.; Agarwal, R. One-Dimensional Polaritons with Size-Tunable and Enhanced Coupling Strengths in Semiconductor Nanowires. *Proc. Natl. Acad. Sci. U. S. A.* **2011**, *108*, 10050−10055.
(32) Reithmaier, J. P.; Sek, G.; Löffler, A.; Hofmann, C.; Kuhn, S.; Reitzenstein, S.; Keldysh, L. V.; Kulakovskii, V. D.; Reinecke, T. L.; Forchel, A. Strong Coupling in a Single Quantum Dot-Semiconductor Microcavity System. *Nature* **2004**, *432*, 197.
(33) Yamamoto, Y.; Tassone, F.; Cao, H. *Semiconductor Cavity Quantum Electrodynamics*; Springer: Berlin, 2000; p 169.
(34) van Vugt, L. K.; Rühle, S.; Ravindran, P.; Gerritsen, H. C.; Kuipers, L.; Vanmaekelbergh, D. Exciton Polaritons Confined in a ZnO Nanowire Cavity. *Phys. Rev. Lett.* **2006**, *97*, 147401.
(35) Du, W.; Zhang, S.; Shi, J.; Chen, J.; Wu, Z.; Mi, Y.; Liu, Z.; Li, Y.; Sui, X.; Wang, R.; Qiu, X.; Wu, T.; Xiao, Y.; Zhang, Q.; Liu, X. Strong Exciton−Photon Coupling and Lasing Behavior in All-Inorganic CsPbBr3Micro/Nanowire Fabry-Pérot Cavity. *ACS Photonics* **2018**, *5*, 2051−2059.

DOI: 10.1021/acsnano.8b02793
ACS Nano 2018, 12, 6170−6178

(36) Zhang, S.; Shang, Q.; Du, W.; Shi, J.; Wu, Z.; Mi, Y.; Chen, J.; Liu, F.; Li, Y.; Liu, M.; Zhang, Q.; Liu, X. Strong Exciton-Photon Coupling in Hybrid Inorganic-Organic Perovskite Micro/Nanowires. *Adv. Opt. Mater.* **2018**, *6*, 1701032.
(37) Evans, T. J. S.; Schlaus, A.; Fu, X.; Zhong, T. L.; Atallah, M. S.; Spencer, L. E.; Brus, S.; Jin, X.-Y.; Zhu. Continuous-Wave Lasing in Cesium Lead Bromide Perovskite Nanowires. *Adv. Opt. Mater.* **2018**, *6*, 1700982.
(38) Tsivion, D.; Schvartzman, M.; PopovitzBiro, R.; von Huth, P.; Joselevich, E. Guided Growth of Millimeter-Long Horizontal Nanowires with Controlled Orientations. *Science* **2011**, *333*, 1003−7.
(39) Shoaib, M.; Zhang, X.; Wang, X.; Zhou, H.; Xu, T.; Wang, X.; Hu, X.; Liu, H.; Fan, X.; Zheng, W.; Yang, T.; Yang, S.; Zhang, Q.; Zhu, X.; Sun, L.; Pan, A. Directional Growth of Ultralong CsPbBr3 Perovskite Nanowires for High-Performance Photodetectors. *J. Am. Chem. Soc.* **2017**, *139*, 15592−15595.
(40) Zhou, H.; Yuan, S.; Wang, X.; Xu, T.; Wang, X.; Li, H.; Zheng, W.; Fan, P.; Li, Y.; Sun, L.; Pan, A. Vapor Growth and Tunable Lasing of Band Gap Engineered Cesium Lead Halide Perovskite Micro/Nanorods with Triangular Cross Section. *ACS Nano* **2017**, *11*, 1189.
(41) Vugt, L. K. V. *Optical Properties of Semiconducting Nanowires*; Utrecht University, 2007.
(42) Pan, A.; Liu, D.; Liu, R.; Wang, F.; Zhu, X.; Zou, B. Optical Waveguide through CdS Nanoribbons. *Small* **2005**, *1*, 980−3.
(43) Pan, A.; Wang, X.; He, P.; Zhang, Q.; Wan, Q.; Zacharias, M.; Zhu, X.; Zou, B. Color-Changeable Optical Transport through Se-Doped CdS 1D Nanostructures. *Nano Lett.* **2007**, *7*, 2970−2975.
(44) Rühle, S.; van Vugt, L. K.; Li, H. Y.; Keizer, N. A.; Kuipers, L.; Vanmaekelbergh, D. Nature of Sub-Band Gap Luminescent Eigenmodes in a ZnO Nanowire. *Nano Lett.* **2008**, *8*, 119.
(45) Van Vugt, L. K.; Piccione, B.; Agarwal, R. Incorporating Polaritonic Effects in Semiconductor Nanowire Waveguide Dispersion. *Appl. Phys. Lett.* **2010**, *97*, 7800.
(46) Kiselev, V. A.; Razbirin, B. S.; Uraltsev, I. N. Additional Waves and Fabry-Perot Interference of Photoexcitons (polaritons) in Thin II−VI Crystals. *Phys. Status Solidi B* **1975**, *72*, 161−172.
(47) van Vugt, L. K.; Zhang, B.; Piccione, B.; Spector, A. A.; Agarwal, R. Size-Dependent Waveguide Dispersion in Nanowire Optical Cavities: Slowed Light and Dispersion Less Guiding. *Nano Lett.* **2009**, *9*, 1684.
(48) Rui, S.; Diederichs, C.; Wang, J.; Liew, T. C. H.; Zhao, J.; Sheng, L.; Xu, W.; Chen, Z.; Xiong, Q. Room Temperature Polariton Lasing in All-Inorganic Perovskite Nanoplatelets. *Nano Lett.* **2017**, *17*, 3982−3988.

DOI: 10.1021/acsnano.8b02793
ACS Nano 2018, 12, 6170−6178